DOI: 10.1002/((please add manuscript number))

Article type: Communication

Versatile Sequential Casting Processing for Highly Efficient and Stable Binary Organic Photovoltaics

Chengliang He, Youwen Pan, Baohua Wu, Xinxin Xia, Zeng Chen, Haiming Zhu, Chang-Qi Ma, Xinhui Lu, Wei Ma, Guanghao Lu, Lijian Zuo and Hongzheng Chen**

C. He, Y. Pan, Prof. L. Zuo, Prof. H. Chen

State Key Laboratory of Silicon Materials, MOE Key Laboratory of Macromolecular Synthesis and Functionalization, International Research Center for X Polymers, Department of Polymer Science and Engineering, Zhejiang University, Hangzhou 310027, P. R. China.
*E-mail: zjuzlj@zju.edu.cn, hzchen@zju.edu.cn.

Prof. G. Lu
Frontier Institute of Science and Technology, Xi'an Jiaotong University, Xi'an 710054, P. R. China.

B. Wu, Prof. W. Ma

State Key Laboratory for Mechanical Behavior of Materials, Xi'an Jiaotong University, Xi'an 710049, P. R. China.

X. Xia, Prof. X. Lu

Department of Physics, Chinese University of Hong Kong, New Territories, Hong Kong 999077, P. R. China.

Prof. C.-Q. Ma

i-Lab & Printable Electronics Research Centre, Suzhou Institute of Nano-tech and Nano-bionics, Chinese Academy of Sciences, Suzhou 215123, P. R. China.

Z. Chen, Prof. H. Zhu

Department of Chemistry, Zhejiang University, Hangzhou 310027, P.R. China.

Keywords: organic solar cell, bulk-heterojunction, sequential casting, binary device, phase-separation

Forming an ideal bulk heterojunction (BHJ) morphology is a critical issue governing the photon to electron process in organic solar cells (OSCs). Complementary to the widely-used blend casting (BC) method for BHJ construction, the sequential casting (SC) can also enable similar or even better morphology and device performance for OSCs. Here we utilize BC and SC methods on three representative donor:acceptor (D:A) blends, *i.e.*, PM6:$PC_{71}BM$, PM6:IT-4F and PM6:L8-BO. We achieve higher power conversion efficiencies (PCEs) in all

cases by taking advantage of beneficial morphology from SC processing, and a champion PCE of 18.86% (certified as 18.44%) based on PM6:L8-BO blend is reached, representing the record value among binary OSCs. The observations on phase separation and vertical distribution inspire the proposal of the swelling-intercalation phase-separation model to interpret the morphology evolution during the SC processing. Further, we find the vertical phase segregation delivers the improvement of device performance via affecting the charge transport and collection processes, as evidenced by the D:A ratio dependent photovoltaic properties. Besides, OSCs based on SC processing show advantages on device photostability and up-scale fabrication. This work demonstrates the versatility and efficacy of SC method for BHJ-based OSCs.

Introduction

Organic solar cells (OSCs) have aroused the enthusiasm of researchers and achieved rapid development in the past a few decades, due to their advantages of superior flexibility, good selective absorption for transparency, lightweight, low-cost production via solution processing, etc.[1-6] The device structure of OSCs consists of a layered structure with an active layer sandwiched between cathode and anode, as buffered by the interfacial charge-transporting layers. The active layer is the most important ingredient to function as the light-absorbing, charge generating and transporting layer. The most popular and efficient active layer structure consists of a donor:acceptor (D:A) blend film with a very tricky nanoscale phase-separated interpenetrating network, or the so-called "bulk heterojunction (BHJ) structure",[7] in order to conquer the high exciton binding energy and bipolar charge-transporting limitations and enable fast exciton dissociation and smooth charge transport, respectively.[8] The rapid progress in molecule design, morphology control, device engineering, *etc.* has greatly boosted the device performance of OSCs to make them more competitive with their inorganic counterparts.[9-25] Currently, record power conversion efficiencies (PCEs) of 19.6% and 20.2% have been achieved for single-junction ternary device and tandem device, respectively.[26,27]

Among all of the factors governing the photon to electron process in OSCs, forming an ideal BHJ morphology is the trickiest one, which requires not only proper D:A pair with

critical miscibility, but also delicate control on the phase-separation kinetics.[8] Constructing BHJ includes two main methods: bottom-to-top bulk phase separation and top-to-bottom permeation. Usually, the active layer is processed by blend casting (BC), where the donor and acceptors are well pre-mixed in solution.[28] The thin solid film is formed by evaporating solvent from the wet film, as accompanied with phase-separation, which is mediated by the choice of solvent and processing conditions. Complementary to the above-mentioned BC method, the sequential casting (SC), also known as layer-by-layer processing, in which the donor and acceptor are deposited sequentially, provides an avenue for morphology control aiming at ordered molecular packing through top-to-bottom permeation.[29-32] The first layer undergoes solvent evaporation to form a crystalline film, which could be adjusted by the solvent choice and drying time. The second layer permeates into the first layer to form a phase-separated structure, which is dictated by the crystallinity and miscibility between the donor and acceptor. It is interesting to observe that the devices processed with SC exhibit similar or even better device performance.[17,33-37] Sun *et al.* combined the fibril network layer and the two-step sequential deposition method to control morphology, which is insensitive to the polymer batches with a higher PCE than that of BC.[33] Jen *et al.* reported that a pseudo-bilayer architecture processed by SC possesses longer exciton diffusion length benefited from higher film crystallinity, thus achieving a higher PCE.[34] Our group combined the SC procedure and the ternary strategy to fabricate device and achieved the highest efficiency at the time.[17] Besides, researchers found that SC shows advantages in

blade-coating procedure and up-scale fabrication.[35,36] Nevertheless, the mechanism underlying how does the SC processing enable the ideal BHJ morphology is still unclear, as well as how will the featured morphology processed with SC affects the optoelectronic properties of OSCs. This further hinders the discovery of more delicate control on the processing to fully explore the potential of SC for high performance.

To address this issue, here we have studied the effect of SC processing on three representative D:A blends, *i.e.*, PM6:$PC_{71}BM$, PM6:IT-4F and PM6:L8-BO, which cover the record material systems within the past dozen years,[38-40] and compared them with the conventional BC processing. Through the multidimensional morphology observations from resonant soft X-ray scattering (RSoXS), grazing-incidence wide-angle X-ray scattering (GIWAXS), atomic force microscopy (AFM), film-depth-dependent light absorption spectroscopy (FLAS) and depth-profiling X-ray photoelectron spectroscopy (D-XPS), *etc.*, it is interesting to find that the SC processing yields BHJ structure with similar phase domains, film crystallinity, and vertical phase-segregation, but more delicate nanoscale phase-separated interpenetrating network when compared to BC processing, while countering to the intuitive understanding of acceptor permeating from top to bottom, *e.g.*, the vertical phase segregation of acceptor actually can be richer at the bottom with SC processing.[41,42] These observations inspire us to propose the swelling-intercalation phase-separation (SIPS) model to interpret the morphology evolution during the SC processing. Further, we studied

the effect of vertical phase separation on the charge collection of OSCs, and find the composition-dependent electron and hole carrier mobility determines the efficacy of vertical phase separation for charge transporting and collection. By taking advantage of beneficial morphology from SC processing, a champion PCE of 18.86% (certified as 18.44%) for PM6:L8-BO blend is reached, as is higher than that of BC processed one. Notably, this result also represents the record value among binary OSCs, and demonstrates the potential of SC method for high-performance OSCs. We then applied the SC processing in up-scaled device, and reached a high efficiency of 16.50%. In addition to the PCE increment, the device photostability is also improved with SC processing.

Results and Discussion

Device Performance

First, we studied the efficacy of SC processing on device performance of OSCs. Three representative material systems, *i.e.*, PM6 as donor to blend with acceptor of $PC_{71}BM$, IT-4F and L8-BO, respectively, are selected by considering their record performance in the past dozen years.[38-40] The chemical structures of these materials are depicted in **Figure 1a**. All of them have been demonstrated to form good BHJ structure with BC processing. The energy levels determined by cyclic voltammetry and absorption profiles of these materials are shown

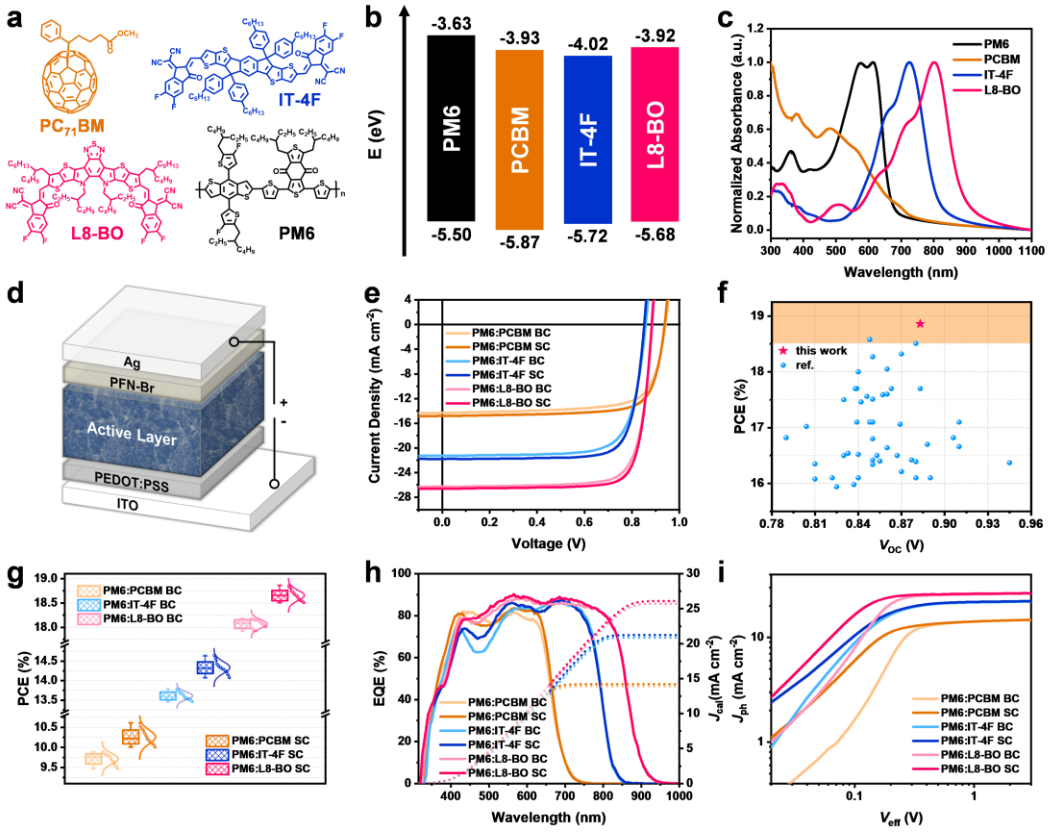

Figure 1. a) Chemical structures of $PC_{71}BM$, IT-4F, L8-BO and the polymer donor PM6. b) Energy level diagram determined by cyclic voltammetry. c) UV-vis absorption spectra of the materials in films. d) A schematic illustration of the conventional device structure. e) *J-V* curves of the optimal devices. f) Comparison of binary devices between this work and references (original data were summarized in **Table S14**). g) PCE statistics of 30 cells for each D:A system. h) EQE curves of the optimal devices. i)

in **Figures 1b**, **1c** and **S1**. Herein, the devices with a conventional structure of ITO/PEDOT:PSS/Active Layer/PFN-Br/Ag were adopted to examine the effect of different processings on device performance (**Figure 1d**). The BC-type devices were fabricated via spin-coating from mixed D:A solution, while the SC-type devices were fabricated via spin-coating from PM6 solution and acceptor solution in sequence. Detailed device fabrication conditions and characterizations are provided in supporting information (**SI)** and summarized in **Tables S1-S4**. **Figure 1e** shows the current density-voltage (*J*-*V*) curves of PM6:$PC_{71}BM$, PM6:IT-4F and PM6:L8-BO blends in BC-type device and SC-type device. Detailed photovoltaic parameters are summarized in **Table 1**. For the best-performing PM6:L8-BO system, the BC-type device exhibits an open-circuit voltage (V_{oc}) of 0.885 V, a short-circuit current density (J_{sc}) of 26.25 mA cm^{-2} and a fill factor (*FF*) of 78.47%, leading to a PCE of 18.18%. When utilizing the SC processing way, the J_{sc} (26.61 mA cm^{-2}) and the *FF* (80.39%) were improved with V_{oc} (0.883 V) almost unchanged (we investigated the luminescence abilities through electroluminescence quantum efficiency (EQE_{EL}) of the devices processed by BC and SC methods (**Figure S2**), and the values are very close), yielding a PCE of 18.86%. Notably, the PCE of 18.86% is the highest among binary OSCs up to data (**Figure 1f**). Besides, the PCE improvement obtained by SC processing is also found in PM6:$PC_{71}BM$ and PM6:IT-4F systems (**Figure 1e** and **Table 1**). It is interesting to observe that the SC processing can generally enable better device performance for OSCs. And a general trend can be derived that both of *FF* and J_{sc} get enhanced, while the V_{oc} slightly

decreases with SC processing, compared to those of BC processing. As a result, it is argued that the SC might be a more superior processing method for high-performance OSCs. Further, the best-performing device is sent to a third authority for certification, and a certified efficiency of 18.44% from National Institute of Metrology (NIM), China was obtained for the best-performing SC-type encapsulated device (**Table 1** and certification report in **SI**). It is worthy to note that this result is the highest among the certified binary OSCs. This further confirms the superiority of SC processing for OSCs.

Table 1. Photovoltaic parameters of the optimal devices.

Active Layer	V_{oc} **(V)**	J_{sc} **(mA cm^{-2})**	J_{cal} **(mA cm^{-2})**[a]	*FF* (%)	**PCE (%)**[b]
PM6:$PC_{71}BM$ (BC)	0.942 (0.942±0.005)	14.32 (14.15±0.14)	13.90	73.33 (72.82±0.54)	9.89 (9.71±0.13)
PM6:$PC_{71}BM$ (SC)	0.938 (0.941±0.006)	14.81 (14.48±0.19)	14.20	76.58 (75.46±0.80)	10.61 (10.26±0.17)
PM6:IT-4F (BC)	0.858 (0.861±0.002)	21.28 (21.00±0.18)	20.87	75.47. (75.34±0.42)	13.78 (13.61±0.10)
PM6:IT-4F (SC)	0.853 (0.852±0.002)	21.75 (21.44±0.27)	21.24	78.85 (78.44±0.60)	14.65 (14.33±0.15)
PM6:L8-BO (BC)	0.885 (0.884±0.002)	26.25 (26.20±0.14)	25.72	78.47 (78.24±0.33)	18.18 (18.06±0.09)
PM6:L8-BO (SC)	0.883 (0.881±0.003)	26.61 (26.61±0.14)	26.10	80.39 (79.74±0.33)	18.86 (18.65±0.10)
PM6:L8-BO (SC)	0.881	26.52		79.0	18.44 [c]

[a] Integrated current density from EQE curve.

[b] Average PCE from 30 devices.

[c] Certified by NIM, China.

To confirm the PV performance variations with different processing, we fabricated more devices to extract and compare the average values and standard deviations of device parameters. **Figure 1g** and **Table 1** provide the PCE statistics from 30 devices for each system. The statistical PCE distributions of all the three systems indicate that the SC-type devices show better performance than the BC-type devices and the variation trend of averaged device parameter is the same as the champion ones, confirming that the SC method exhibits advantages over the BC method for high device performance.

To figure out the origin of improved J_{sc} with SC processing, the external quantum efficiency (EQE) test was performed (**Figure 1h** and **Table 1**). The integrated values (J_{cal}) from the EQE curves are very close to those from the *J-V* curves, validating the device performance derived from *J-V* measurement. While it is interesting to observe that the shape of EQE actually gets changed from BC to SC processing for PM6:$PC_{71}BM$ and PM6:IT-4F systems, but remains for PM6:L8-BO system. These results suggest that both optical interference and internal carrier dynamics play a role for the improvement in J_{sc}.[34] Further, to understand the mechanism underlying the improved FF with SC processing, we studied the carried dynamics in OSCs by investigating the relationship between photocurrent density and effective voltage of the devices to characterize the bias-dependent charge separation and

collection behavior (**Figure 1i** and **Table S5**).[43] The calculated exciton dissociation efficiencies (P_{diss}s) in BC-type devices are 97.02%, 98.09% and 98.36% for PM6:PC_{71}BM, PM6:IT-4F and PM6:L8-BO systems, respectively, while 97.84%, 98.29% and 98.90% for SC-type devices. The calculated charge collection efficiencies (P_{coll}s) are 83.06%, 83.18% and 89.09% for PM6:PC_{71}BM, PM6:IT-4F and PM6:L8-BO systems, respectively, while 85.12%, 85.03% and 90.56% in SC-type devices. It is found SC-type devices show subtle advantage in P_{diss} and more obvious advantage in P_{coll} compared with BC-type devices, affording to the improved *FF*. As a result, it is argued that the SC processing method is practical and universal for PCE improvement with gain in J_{sc} and *FF* via changing both the light trapping properties and the carrier dynamics.

Film Morphology

Considering that the different processing mostly affects the morphology of the active layer, we put emphasis on resolving the film morphology characteristics of these systems with different processing. First, we conducted RSoXS tests to analyze the phase separation (**Figures 2a**, **S3** and **Table S6**), which can give information on the phase separation size and phase purity.[44,45] These parameters are essentially important for charge generation and charge transport, as unveiled in previous work.[44] For PM6:PC_{71}BM system, the difference in phase purity between the BC-type and SC-type films is negligible, and the average phase domain size of the SC-type film is 13.36 nm, which is smaller than that from BC processing

(14.70 nm). For non-fullerene systems (PM6:IT-4F and PM6:L8-BO), it is interesting to observe that the phase purity of SC-type film is lower than that of BC-type. The average domain sizes decrease from 20.98 nm to 19.10 nm for PM6:L8-BO system, but increased from 17.96 nm to 21.93 nm for IT-4F system with SC processing. The phase domain size of all the above systems seems to be within the range of exciton diffusion for efficient exciton separation or charge generation. Intuitively, during the SC processing, the acceptor will permeate into PM6 from top to bottom, and thus is expected to form a purer grain due to the pre-formed pristine PM6 film. As a result, it is counter-intuitive to observe the reduced phase purity during the SC processing, according to the infiltration process. Instead, the phase purity seems to be more closely related to other parameters than the "permeation" process.

GIWAXS characterization was performed to investigate the molecular packing and the crystalline properties.[46] As shown in **Figures 2b-2c**, **S4** and **Table S7**, there is no significant difference between BC-type and SC-type films in the in-plane direction. In the out-of-plane direction, for the PM6:$PC_{71}BM$ system, its diffraction peaks in SC-type film are not as sharp as observed in BC-type film (q_z = 1.31 $Å^{-1}$ (d = 4.79 Å) and q_z = 1.68 $Å^{-1}$ (d = 3.74 Å)). For

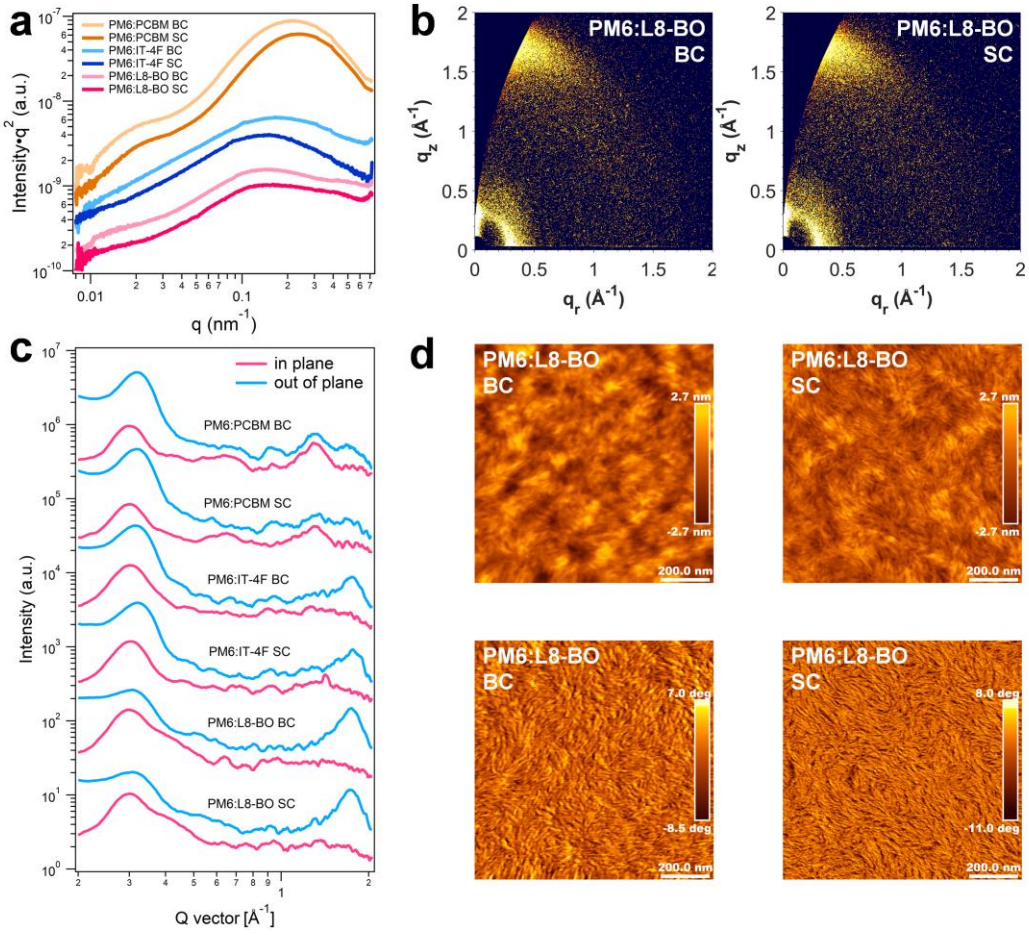

Figure 2. a) RSoXS profiles of the blend films based on different process condition. b) 2D GIWAXS images of PM6:L8-BO blend films from BC and SC methods. c) GIWAXS intensity profiles of the three blend films along the in-plane (blue lines) and out-of-plane (red lines) directions. d) AFM height (top) and phase (bottom) images of PM6:L8-BO blend films from BC and SC methods.

the PM6-IT-4F system, the π-π stacking becomes denser in SC-type film, with diffraction peak located at q_z = 1.74 Å^{-1} (d = 3.61 Å) in BC-type film and q_z = 1.77 Å^{-1} (d = 3.55 Å) in SC-type films. Besides, SC-type film presents slightly larger crystal correlation length (CCL) (35.8 Å) than BC-type film (34.1 Å). For the PM6:L8-BO system, no obvious change in the stacking distance (d = 3.63 Å) and a small increase in the CCL (28.3 Å *vs.* 26.3 Å) were obtained from BC-type film to SC-type film. In general, for fullerene and non-fullerene systems, the overall difference between the films obtained by the two processing methods in GIWAXS is not very obvious, suggesting the film phase-separation might be similar with SC and BC processing ways. The difference may exist in the interaction of solvent/acceptor with donor during SC process.

AFM measurement was conducted to study the surface morphology. Combining the height and phase images shown in **Figures 2d** and **S6-S7**, we found that nanofiber-like morphology could be observed in all the three blends, indicating the well-formed interpenetrating networks. The similar fibrillar network structure was also reported in polymer donor D18 based active layer.[47,48] Particularly, it is found that a more delicate nanoscale phase-separated interpenetrating network is formed through SC method (**Figure S8**). These results can be attributed to the intercalation of acceptor to the donor after solvent swelling during SC process. In addition, we tested the pristine D/A film as shown in **Figure S7**. It is found the surface of the acceptor is relatively rough, and the texture of the donor

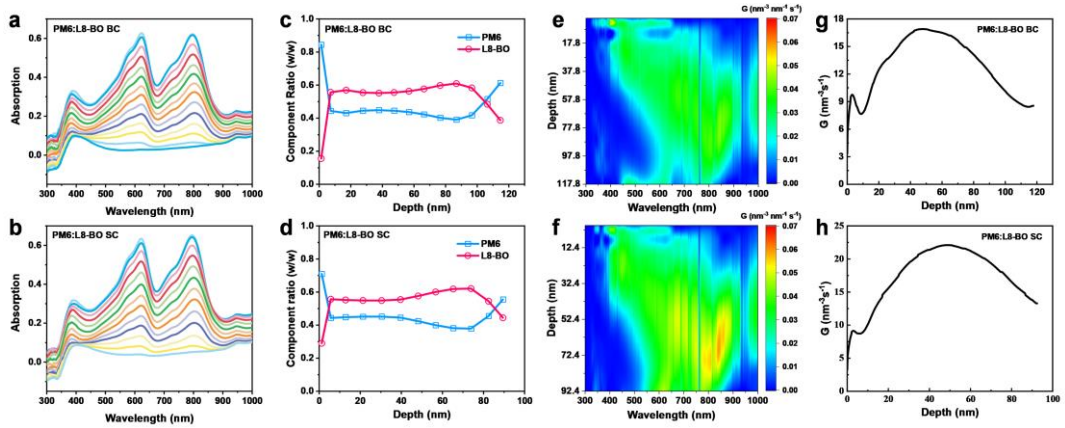

Figure 3. a–b) Film-depth-dependent light absorption spectra of BC-type and SC-type films in PM6:L8-BO system. c–d) Components distribution profiles at different film-depths. The calculated exciton generation contours in (e) BC-type films and (f) SC-type films. g–h) Film-depth-dependent exciton generation rates as obtained by integration of (e) and (f) along the wavelength direction.

could be enhanced after being swelled by chloroform due to that the amorphous regions of lower density in a semi-crystalline polymer film are more susceptible to swelling than the crystalline regions[17,29], which could lay the foundation for the formation of delicate interpenetrating network in the SC blend films.

To further investigate the difference in the vertical phase segregation, which has been demonstrated the major difference for films processed from BC and SC, we performed the FLAS and the detailed calculations could be found in **SI** (**Figures 3** and **S9-S12**).[49-51] FLAS of BC-type and SC-type films of PM6:L8-BO blend are displayed in **Figures 3a** and **3b**. **Figures 3c** and **3d** provide the components distribution profiles at different film-depths to give a re-aligned sight of D:A content for clarity and we combined them in the same figure

for clearer comparison in **Figure S12a**. It can be found that PM6 and L8-BO show obvious inhomogeneous distribution along the vertical direction for both BC and SC processed films. For both cases, the PM6 enriches at both top and bottom interface. However, it is observed that the SC processed film has less PM6 enrichment at both interfaces. In addition, it is also found that PM6 enriches at both top and bottom interfaces in the two processing cases for PM6:IT-4F system (**Figure S10**). For PM6:$PC_{71}BM$ system (**Figure S9**), in the BC-type films the acceptor enriches at both top and bottom interfaces, while in the SC-type film, PM6 at both ends tends to converge towards the middle. Interestingly, vertical distributions in all the three systems are contrast to conventional cognition that the formation of vertical phase-separated structures with D/A enrichment at both electrodes in sequential deposition process for both fullerene and non-fullerene-based systems.[41,42] We then performed the D-XPS to investigate the relative D:A ratio along with depth throughout the whole film. Taking the best-performing PM6:L8-BO system for example, since both PM6 and L8-BO contain fluorine (F), while only L8-BO contains nitrogen (N), we attribute the F element to both PM6 and L8-BO, N element to only L8-BO. Based on the F/N atom ratio, the polymer weight content ($D_{wt\%}$) at different depths can be calculated as shown in **Figures S13-S14 and Tables S8-S9**. Detailed calculation method could be found in the note of **Figure S13**. For PM6:L8-BO films from BC and SC processing, the PM6 enriches at both top and bottom interfaces. It can be inferred that the D-XPS results are in consistent with the FLAS results (**Figure 3**) to a certain extent.

Figures 3e and **3f** show the distribution of charge generation intensity (exciton generation rate) within the photovoltaic devices, which is numerically simulated from the FLAS in combination with a modified transfer-matrix optical model.[50] The excitons are mainly generated at the center and the bottom of the blend films. Particularly, the density of exciton in the SC-type film is much higher than that of the BC-type film in the region from 600 to 900 nm, which contributes to the improved EQE and J_{sc}. According to **Figure 3f**, L8-BO with an absorption peak around 800 nm contributes more to the exciton generation relative to PM6 with an absorption edge around 600 nm, which agrees well with the composition distribution extracted from the FLAS.

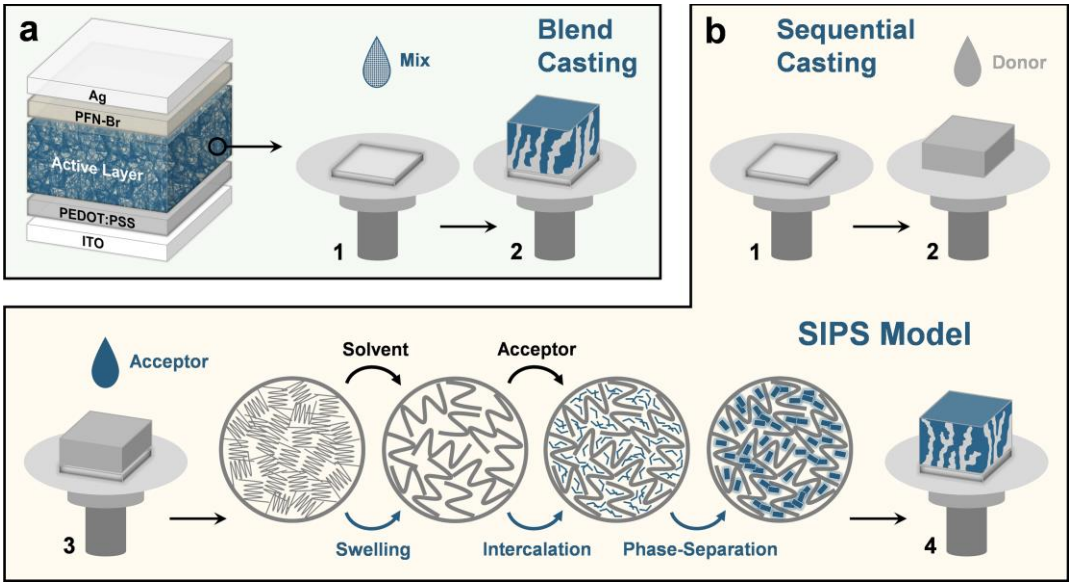

Figure 4. a) Diagram of fabrication procedures for BC-type devices. b) Diagram of fabrication procedures for SC-type devices and the proposed swelling-intercalation-phase separation (SIPS) model.

The counter-intuitive phenomena observed above, *e.g.*, the phase purity and vertical phase segregation, suggest a different process dominating the phase-separation kinetics rather than the inter-filtration of acceptor from top to bottom. Considering that the formed morphology with SC processing is actually a perfect BHJ structure compared to BC (**Figure 4a**), a phase-separation process resembles to BC should occur during the SC processing. Here, we propose the SIPS model to interpret the whole process, as shown in **Figure 4b**. With depositing the acceptor solution onto the PM6 film, the solvent, *i.e.*, chloroform, will first swell PM6 polymer to form a gel-like structure. Following this, the acceptor molecules

will intercalate into the swollen polymer matrix to form a well-mixed wet blend film. Finally, during the solvent evaporation, the phase-separation will occur in the well-mixed donor-acceptor blend film. As a result, the SC will undergo similar phase-separation and yield similar morphology to the BC processing. This model well explains the formation of very good BHJ and the general observation on the efficacy of SC for high-performance OSCs. Moreover, this model explains the counter-intuitive observation on phase purity and vertical phase segregation, which are determined by the miscibility between the donor and acceptor,[17] and the solvent permeation and evaporation kinetics.[28] According to the SIPS model, the solvent will first "swell" the pristine polymer, and this composes an exact solvent selection criterion for solvent: the solubility and boiling point must be in a proper range. This has been confirmed by using different processing solvents with different boiling point (BP) and solubility for BC and SC processing (**Figures 5a-5b, S15-S16** and **Tables S2-S4**, **S10-S12**). For example, by selecting the tetrahydrofuran (THF), which shows comparable BP but low solubility compared to chloroform (CF), obvious drop in PCE is observed, as attributed to the poor swelling process (**Figure 5b** and **Table S11**). By using chlorobenzene (CB) showing similar solubility but higher BP compared to CF, the long dwelling time of CB could over-react with the PM6 layer to form a dense solution layer rather than a swelling polymer matrix, and thus cause poor morphology and low device performance (**Figure 5b** and **Table S11**). Compromising the BP and solubility, the toluene (Tol) recovers most of the efficiency compared to THF and CB. Further, a poor efficiency is expected when using an

even high BP solvent, *i.e.*, o-Xylene (*o*-XY) (**Figure 5b** and **Table S11**). These observations well support the SIPS model, and confirm the above solvent selection rule derived from SIPS model (more detailed analysis can be found in **SI**, **Solvent Selection Rules** Section).

Composition dependent carrier dynamics

We observe that the improved device performance is partially attributed to the increased *FF* (statistics in **Figure S17a** and **Table 1**), which is closely related to the carrier dynamics and subsequently the morphology. Considering the lateral phase-separated morphology for films processed from SC and BC is actually within the optimal ranges, we focus on the effect of vertical phase segregation on the carrier dynamics, and pay particular attention on the ratio dependent photovoltaic properties. Hence, we chose the best-performing PM6:L8-BO blend as the object and selected the D:A ratios of four representative positions (1:0.4, 1:0.8, 1:1.2 and 1:1.6 by wt.) according to its vertical distribution characteristics (**Figure S12b**) to fabricate the device for charge dynamic study. **Figure 5c** shows the *J*-*V* curves of the BC-type devices based on different D:A ratios and the SC-type device. Detailed photovoltaic parameters are summarized in **Table 2**. The BC-type devices deliver PCEs of 6.51%, 18.04%, 18.18% and 17.70% for the ratio of 1:0.4, 1:0.8, 1:1.2 and 1:1.6, repectively. **Figure S17b** provides the EQE curves of the corresponding devices. It can be inferred that the ratio of 1:1.2 is the best for device operation and this ratio occupies the largest proportion in the vertical distribution.

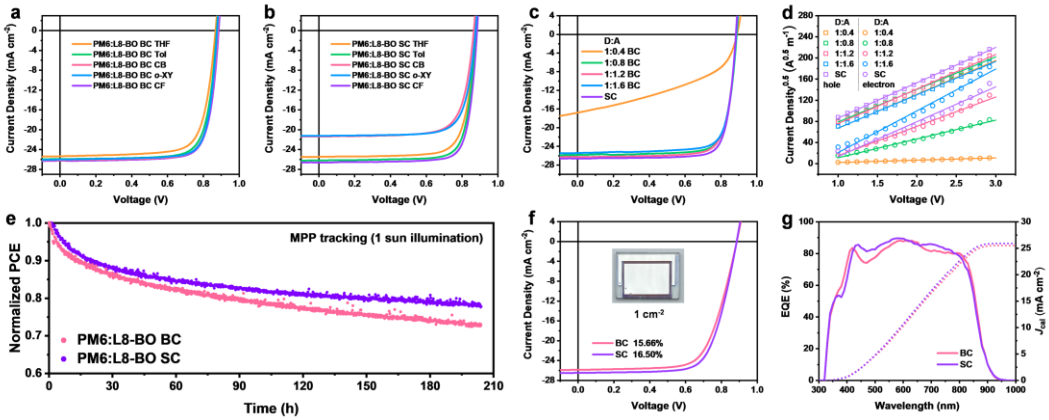

Figure 5. a) *J-V* curves of the optimal devices based on PM6:L8-BO system processed via BC method with different solvents. b) *J-V* curves of the optimal devices based on PM6:L8-BO system processed via SC method with different solvents. c) *J-V* curves of the optimal devices based on PM6:L8-BO system processed via BC and SC methods. d) Charge carrier mobility of the optimal devices based on PM6:L8-BO system processed via BC and SC methods. e) Photostability comparison between BC-type and SC-type devices based on PM6:L8-BO system. f) *J-V* curves of the optimal 1 cm^2 devices based on PM6:L8-BO system. g) EQE curves of the optimal 1 cm^2 devices based on PM6:L8-BO system.

As shown in **Figure S17c**, the SC-type device possesses the highest P_{diss} and P_{coll} values (98.90% and 90.56%), while the BC-type device under 1:0.4 ratio exhibts the worst P_{diss} and P_{coll} values (72.92% and 43.24%). Charge separation and collection behaviors are less affected with the D:A ratios ranging from 1:0.8 to 1:1.6. To investigate the charge transport after charge separation, the space-charge-limited current (SCLC) method was utilized to examine the charge carrier mobility in the blends (**Figure 5d** and **Table 2**). In BC-type devices, with the increase of the acceptor ratio, the electron mobility increases gradually, while the hole mobility remains basically unchanged. Among them, the value of μ_e/μ_h for device based on 1:1.2 ratio is the closest to 1, indicating that the charge transport is the most balanced. This suggests that vertical phase-segration affects the carrier dynamics by

influencing the electron collection properties. Compared with the BC-type device under 1:1.2 ratio, the SC-type device exhibits a slightly higher mobility, and its value of μ_e/μ_h is 1.03. It can be seen from **Figure 3h** that the SC-type film has the highest exciton density in the middle, with the extremely balanced mobility, it is favorable to improve the device performance.

Further, the charge recombination behavior was then investigated by light intensity (P_{light}) dependent J_{sc} and V_{oc}.[52] As shown in **Figure S17d**, from the *n* values derived from the P_{light} dependent V_{oc}, it is suggested that monomolecular recombination is the dominant recombination type and the BC-type device under 1:0.4 ratio suffers monomolecular recombination severely. The α values of current density versus P_{light} indicate that the SC-type device can suppress the trap-mediated monomolecular charge recombination and facilitate the charge extraction, and this contributes to the high J_{sc} and *FF*. The suppress recombination is also consistent with the balanced charge transport mentiond above.

Stability is an important indicator to quantify the device[53] and previous work demonstrated that SC processed devices show improved thermal stability, which is benefited from the formation of the robust polymer network during SC process.[29,54,55] In order to get closer to the application scenario, we tested the photo-stability under MPP conditions and found that SC-type devices showed advantages (**Figures 5e** and **S18-S22**). Since the storage stability in nitrogen atmosphere of the two types encapsulated devices differs slightly (**Figure**

S19), it is argued that the influence of light may be the main cause and we carried out photoaging experiments (**Figures S20-S22)**. It is found that the intrinsic stability of PM6 film and the pristine IT-4F are the poorest among all the pristine and blend films. For the blend films, the donor and acceptor of the PM6:IT-4F system is greatly affected simultaneously, while the donors in the PM6:$PC_{71}BM$ and PM6:L8-BO systems experience more severe decay compared with acceptors. It is also found that the SC-type films show a subtle advantage in photoaging process (**Figure S22**). Based on the SIPS model, the amorphous and semi-crystalline regions in polymer film are more susceptible to swelling, and a more delicate interpenetrating network is finally formed in SC processing. Therefore, we correlate the better photostability of SC-processed films with the swollen donor region and the more delicate D:A interpenetrating network. To further demonstrate the superiority of the SC processing method, we fabricated the large area (1 cm^2) devices (**Figure 5f**). The results show that the SC-type device exhibits higher J_{sc} and *FF* (**Table S13**), leading to a higher PCE (16.50%) than that of BC-type device (15.66%). In addition, the response ranges that achieve EQE gain (**Figure 5g**) are very similar to that in **Figure 2g**. This indicates that the SC processing has certain prospects for up-scaled device fabrication.

Table 2. Photovoltaic parameters of the optimal devices based on different device types and different D:A ratios.

Active Layer	V_{oc} (V)	J_{sc} (mA cm^{-2})	*FF* (%)	PCE (%)	μ_e[a] (10^{-4} cm^2 V^{-1} s^{-1})	μ_h[b] (10^{-4} cm^2 V^{-1} s^{-1})

PM6:L8-BO BC (1:0.4)	0.890	16.78	43.76	6.51	0.0622	13.8
PM6:L8-BO BC (1:0.8)	0.888	25.84	78.82	18.04	4.24	12.7
PM6:L8-BO BC (1:1.2)	0.885	26.25	78.47	18.18	10.3	14.3
PM6:L8-BO BC (1:1.6)	0.885	25.42	78.70	17.70	21.0	13.3
PM6:L8-BO SC	0.883	26.61	80.39	18.86	14.6	15.0

[a] Electron mobility from SCLC method.

[b] Hole mobility from SCLC method.

Conclusion

In summary, we have demonstrated the versatility and efficacy of sequential casting method for fabricating BHJ-based OSCs with diverse D:A pairs, *i.e.*, PM6:$PC_{71}BM$, PM6:IT-4F and PM6:L8-BO. Improvement in device performance has been generally observed in all cases. Particularly, the SC method enables a record efficiency of 18.86% for PM6:L8-BO solar cells (certified as 18.44%), and this represents the best-performing D:A binary OSC, demonstrating the effectiveness of sequential deposition for device optimization. Further, we propose the SIPS model to describe the film formation process during the sequential deposition, and this model well explains some counter-intuitive phase separation

observations. Based on the PM6:L8-BO system, we observe that the vertical phase segregation affects the device performance via affecting the charge transport and recombination processes. These results are helpful in understanding the film morphology evolution and further developing high-performance OSCs.

Supporting Information

Supporting Information is available from the Wiley Online Library or from the author.

Acknowledgments

This work was supported by the National Natural Science Foundation of China (Nos. 21734008, 52173185, 5212780017, 61721005), National Key Research and Development Program of China (Nos. 2019YFA0705900), and Research Start-up Fund from Zhejiang University. RSoXS data were acquired at beamlines 7.3.3 and 11.0.1.2 at the Advanced Light Source, which is supported by the Director, Office of Science, Office of Basic Energy Sciences, of the U.S. Department of Energy under Contract No. DE-AC02-05CH11231. The authors thank Dr. Eric Schaible and Dr. Chenhui Zhu at beamline 7.3.3, and Dr. Cheng Wang at beamline 11.0.1.2 for assistance with data acquisition. The authors are grateful for the technical support for Nano-X from Suzhou Institute of Nano-Tech and Nano-Bionics, Chinese Academy of Sciences.

Received: ((will be filled in by the editorial staff))

Revised: ((will be filled in by the editorial staff))

Published online: ((will be filled in by the editorial staff))

References

[1] O. Inganas, *Adv. Mater.* **2018**, *30*, 1800388.

[2] J. Hou, O. Inganas, R. H. Friend, F. Gao, *Nat. Mater.* **2018**, *17*, 119.

[3] P. Cheng, G. Li, X. Zhan, Y. Yang, *Nat. Photonics* **2018**, *12*, 131.

[4] Y. Li, C. He, L. Zuo, F. Zhao, L. Zhan, X. Li, R. Xia, H. L. Yip, C. Z. Li, X. Liu, H. Chen, *Adv. Energy Mater.* **2021**, *11*, 2003408.

[5] S. Li, C.-Z. Li, M. Shi, H. Chen, *ACS Energy Lett.* **2020**, *5*, 1554.

[6] Q. Shen, C. He, S. Li, L. Zuo, M. Shi, H. Chen, *Acc. Mater. Res.* **2022**, https://doi.org/10.1021/accountsmr.2c00052

[7] G. Yu, J. Gao, J. C. Hummelen, F. Wudl, A. J. Heeger, *Science* **1995**, *270*, 1789.

[8] Y. Huang, E. J. Kramer, A. J. Heeger, G. C. Bazan, *Chem. Rev.* **2014**, *114*, 7006.

[9] L. Zuo, S. B. Jo, Y. Li, Y. Meng, R. J. Stoddard, Y. Liu, F. Lin, X. Shi, F. Liu, H. W. Hillhouse, D. S. Ginger, H. Chen, A. K. Jen, *Nat. Nanotechnol.* **2022**, *17*, 53.

[10] Y. Lin, J. Wang, Z. G. Zhang, H. Bai, Y. Li, D. Zhu, X. Zhan, *Adv. Mater.* **2015**, *27*, 1170.

[11] S. Li, L. Zhan, F. Liu, J. Ren, M. Shi, C. Z. Li, T. P. Russell, H. Chen, *Adv. Mater.* **2018**, *30*, 1705208.

[12] J. Yuan, T. Huang, P. Cheng, Y. Zou, H. Zhang, J. L. Yang, S. Y. Chang, Z. Zhang, W. Huang, R. Wang, D. Meng, F. Gao, Y. Yang, *Nat. Commun.* **2019**, *10*, 570.

[13] J. Yuan, Y. Zhang, L. Zhou, G. Zhang, H.-L. Yip, T.-K. Lau, X. Lu, C. Zhu, H. Peng, P. A. Johnson, M. Leclerc, Y. Cao, J. Ulanski, Y. Li, Y. Zou, *Joule* **2019**, *3*, 1140.

[14] C. He, Z. Chen, T. Wang, Z. Shen, Y. Li, J. Zhou, J. Yu, H. Fang, Y. Li, S. Li, X. Lu, W. Ma, F. Gao, Z. Xie, V. Coropceanu, H. Zhu, J.-L. Bredas, L. Zuo, H. Chen, *Nat. Commun.* **2022**, *13*, 2598.

[15] S. Li, L. Zhan, Y. Jin, G. Zhou, T. K. Lau, R. Qin, M. Shi, C. Z. Li, H. Zhu, X. Lu, F. Zhang, H. Chen, *Adv. Mater.* **2020**, *32*, 2001160.

[16] C. He, Y. Pan, Y. Ouyang, Q. Shen, Y. Gao, K. Yan, J. Fang, Y. Chen, C.-Q. Ma, J. Min, C. Zhang, L. Zuo, H. Chen, *Energy Environ. Sci.* **2022**, https://doi.org/10.1039/D2EE00595F

[17] L. Zhan, S. Li, X. Xia, Y. Li, X. Lu, L. Zuo, M. Shi, H. Chen, *Adv. Mater.* **2021**, *33*, 2007231.

[18] C. He, Z. Bi, Z. Chen, J. Guo, X. Xia, X. Lu, J. Min, H. Zhu, W. Ma, L. Zuo, H. Chen, *Adv. Funct. Mater.* **2022**, *32*, 2112511.

[19] L. Zhan, S. Li, T.-K. Lau, Y. Cui, X. Lu, M. Shi, C.-Z. Li, H. Li, J. Hou, H. Chen, *Energy Environ. Sci.* **2020**, *13*, 635.

[20] S. Li, L. Zhan, C. Sun, H. Zhu, G. Zhou, W. Yang, M. Shi, C. Z. Li, J. Hou, Y. Li, H. Chen, *J. Am. Chem. Soc.* **2019**, *141*, 3073.

[21] Y. Li, Y. Guo, Z. Chen, L. Zhan, C. He, Z. Bi, N. Yao, S. Li, G. Zhou, Y. Yi, Y. Yang, H. Zhu, W. Ma, F. Gao, F. Zhang, L. Zuo, H. Chen, *Energy Environ. Sci.* **2022**, *15*, 855.

[22] C. He, Y. Li, Y. Liu, Y. Li, G. Zhou, S. Li, H. Zhu, X. Lu, F. Zhang, C.-Z. Li, H. Chen, *J. Mater. Chem. A* **2020**, *8*, 18154.

[23] S. Li, L. Zhan, N. Yao, X. Xia, Z. Chen, W. Yang, C. He, L. Zuo, M. Shi, H. Zhu, X. Lu, F. Zhang, H. Chen, *Nat. Commun.* **2021**, *12*, 4627.

[24] L. Zhan, S. Li, Y. Li, R. Sun, J. Min, Z. Bi, W. Ma, Z. Chen, G. Zhou, H. Zhu, M. Shi, L. Zuo, H. Chen, *Joule* **2022**, *6*, 662.

[25] C. He, Y. Li, S. Li, Z. P. Yu, Y. Li, X. Lu, M. Shi, C. Z. Li, H. Chen, *ACS Appl. Mater. Interfaces* **2020**, *12*, 16700.

[26] L. Zhu, M. Zhang, J. Xu, C. Li, J. Yan, G. Zhou, W. Zhong, T. Hao, J. Song, X. Xue, Z. Zhou, R. Zeng, H. Zhu, C. C. Chen, R. C. I. MacKenzie, Y. Zou, J. Nelson, Y. Zhang, Y. Sun, F. Liu, *Nat. Mater.* **2022**, *21*, 656.

[27] Z. Zheng, J. Wang, P. Bi, J. Ren, Y. Wang, Y. Yang, X. Liu, S. Zhang, J. Hou, *Joule* **2022**, *6*, 171.

[28] J. J. van Franeker, M. Turbiez, W. Li, M. M. Wienk, R. A. Janssen, *Nat Commun* **2015**, *6*, 6229.

[29] J. C. Aguirre, S. A. Hawks, A. S. Ferreira, P. Yee, S. Subramaniyan, S. A. Jenekhe, S. H. Tolbert, B. J. Schwartz, *Adv. Energy Mater.* **2015**, *5*, 1402020.

[30] D. H. Kim, J. Mei, A. L. Ayzner, K. Schmidt, G. Giri, A. L. Appleton, M. F. Toney, Z. Bao, *Energy Environ. Sci.* **2014**, *7*, 1103.

[31] S. A. Hawks, J. C. Aguirre, L. T. Schelhas, R. J. Thompson, R. C. Huber, A. S. Ferreira, G. Zhang, A. A. Herzing, S. H. Tolbert, B. J. Schwartz, *J. Phys. Chem. C* **2014**, *118*, 17413.

[32] X. Li, X. Du, J. Zhao, H. Lin, C. Zheng, S. Tao, *Solar RRL* **2020**, *5*, https://doi.org/10.1002/solr.202200076

[33] K. Weng, L. Ye, L. Zhu, J. Xu, J. Zhou, X. Feng, G. Lu, S. Tan, F. Liu, Y. Sun, *Nat. Commun.* **2020**, *11*, 2855.

[34] K. Jiang, J. Zhang, Z. Peng, F. Lin, S. Wu, Z. Li, Y. Chen, H. Yan, H. Ade, Z. Zhu, A. K. Jen, *Nat. Commun.* **2021**, *12*, 468.

[35] Y. Zhang, K. Liu, J. Huang, X. Xia, J. Cao, G. Zhao, P. W. K. Fong, Y. Zhu, F. Yan, Y. Yang, X. Lu, G. Li, *Nat. Commun.* **2021**, *12*, 4815.

[36] R. Sun, Q. Wu, J. Guo, T. Wang, Y. Wu, B. Qiu, Z. Luo, W. Yang, Z. Hu, J. Guo, M. Shi, C. Yang, F. Huang, Y. Li, J. Min, *Joule* **2020**, *4*, 407.

[37] R. Sun, J. Guo, C. Sun, T. Wang, Z. Luo, Z. Zhang, X. Jiao, W. Tang, C. Yang, Y. Li, J. Min, *Energy Environ. Sci.* **2019**, *12*, 384.

[38] M. Zhang, X. Guo, W. Ma, H. Ade, J. Hou, *Adv. Mater.* **2015**, *27*, 4655.

[39] Y. Cui, H. Yao, L. Hong, T. Zhang, Y. Xu, K. Xian, B. Gao, J. Qin, J. Zhang, Z. Wei, J. Hou, *Adv. Mater.* **2019**, *31*, 1808356.

[40] C. Li, J. Zhou, J. Song, J. Xu, H. Zhang, X. Zhang, J. Guo, L. Zhu, D. Wei, G. Han, J. Min, Y. Zhang, Z. Xie, Y. Yi, H. Yan, F. Gao, F. Liu, Y. Sun, *Nat. Energy* **2021**, *6*, 605.

[41] S. Dai, M. Li, J. Xin, G. Lu, P. Xue, Y. Zhao, Y. Liu, M. Sun, L. Yu, Z. Tang, G. Lu, W. Ma, X. Zhan, *J. Mater. Chem. A* **2022**, *10*, 1948.

[42] X. Li, R. Zhu, Z. He, X. Du, H. Lin, C. Zheng, G. Yang, Z. Chen, S. Tao, *ACS Appl. Mater. Interfaces* **2022**, https://doi.org/10.1021/acsami.2c04997

[43] A. K. Kyaw, D. H. Wang, D. Wynands, J. Zhang, T. Q. Nguyen, G. C. Bazan, A. J. Heeger, *Nano Lett.* **2013**, *13*, 3796.

[44] L. Zhang, B. Lin, B. Hu, X. Xu, W. Ma, *Adv. Mater.* **2018**, *30*, 1800343.

[45] J. Zhao, Y. Li, G. Yang, K. Jiang, H. Lin, H. Ade, W. Ma, H. Yan, *Nat. Energy* **2016**, *1*, 15027.

[46] J. Mai, Y. Xiao, G. Zhou, J. Wang, J. Zhu, N. Zhao, X. Zhan, X. Lu, *Adv. Mater.* **2018**, 1802888.

[47] Q. Liu, Y. Jiang, K. Jin, J. Qin, J. Xu, W. Li, J. Xiong, J. Liu, Z. Xiao, K. Sun, S. Yang, X. Zhang, L. Ding, *Sci. Bull.* **2020**, *65*, 272.

[48] Y. Wei, J. Yu, L. Qin, H. Chen, X. Wu, Z. Wei, X. Zhang, Z. Xiao, L. Ding, F. Gao, H. Huang, *Energy Environ. Sci.* **2021**, *14*, 2314.

[49] L. Bu, S. Gao, W. Wang, L. Zhou, S. Feng, X. Chen, D. Yu, S. Li, G. Lu, *Adv. Electron. Mater.* **2016**, *2*, 1600359.

[50] Z. Wang, Y. Hu, T. Xiao, Y. Zhu, X. Chen, L. Bu, Y. Zhang, Z. Wei, B. B. Xu, G. Lu, *Adv. Opt. Mater.* **2019**, *7*, 1900152.

[51] T. Xiao, J. Wang, S. Yang, Y. Zhu, D. Li, Z. Wang, S. Feng, L. Bu, X. Zhan, G. Lu, *J. Mater. Chem. A* **2020**, *8*, 401.

[52] I. Riedel, J. Parisi, V. Dyakonov, L. Lutsen, D. Vanderzande, J. C. Hummelen, *Adv. Funct. Mater.* **2004**, *14*, 38.

[53] Q. Burlingame, M. Ball, Y.-L. Loo, *Nat. Energy* **2020**, *5*, 947.

[54] H. Hwang, H. Lee, S. Shafian, W. Lee, J. Seok, K. Y. Ryu, D. Yeol Ryu, K. Kim, *Polymers* **2017**, *9*, 456.

[55] S. Dong, K. Zhang, B. Xie, J. Xiao, H.-L. Yip, H. Yan, F. Huang, Y. Cao, *Adv. Energy Mater.* **2019**, *9*, 1802832.

Sequential casting (SC) processing is practical and universal for device performance improvement in both fullerene and non-fullerene-based systems of organic solar cells (OSCs). The swelling-intercalation phase-separation model is proposed to interpret the morphology evolution during the SC processing. Notably, a champion efficiency of 18.86% (certified as 18.44%) is reached from SC processing, representing the highest value among binary OSCs.

organic solar cell, bulk-heterojunction, sequential casting, binary device, phase-separation

Chengliang He, Youwen Pan, Baohua Wu, Xinxin Xia, Zeng Chen, Haiming Zhu, Chang-Qi Ma, Xinhui Lu, Wei Ma, Guanghao Lu, Lijian Zuo* and Hongzheng Chen*

Versatile Sequential Casting Processing for Highly Efficient and Stable Binary Organic Photovoltaics